Features of MOG required for recognition by patients with MOG antibody-associated disorders

Caterina Macrini,[1] Ramona Gerhards,[1] Stephan Winklmeier,[1] Lena Bergmann,[2] Simone Mader,[1] Melania Spadaro,[1] Atay Vural,[3] Michaela Smolle,[2,4] Reinhard Hohlfeld,[1] Tania Kümpfel,[1] Stefan F. Lichtenthaler,[5,6] Henri G. Franquelim,[7] Dieter Jenne[8] and Edgar Meinl[1]

Abstract

Antibodies (Abs) to myelin oligodendrocyte glycoprotein (MOG) define a distinct disease entity. Here we aimed to understand essential structural features of MOG required for recognition by autoantibodies from patients. We produced the N-terminal part of MOG in a conformationally correct form; this domain was insufficient to identify patients with MOG-Abs by ELISA even after site-directed binding. This was neither due to a lack of lipid embedding nor to a missing putative epitope at the C-terminus, which we confirmed to be an intracellular domain. When MOG was displayed on transfected cells, patients with MOG-Abs recognized full-length MOG much better than its N-terminal part with the first hydrophobic domain ($p<0.0001$). Even antibodies affinity-purified with the extracellular part of MOG recognized full-length MOG better than the extracellular part of MOG after transfection. The second hydrophobic domain of MOG enhanced the recognition of the extracellular part of MOG by antibodies from patients as seen with truncated variants of MOG. We confirmed the pivotal role of the second hydrophobic domain by fusing the intracellular part of MOG from the evolutionary distant opossum to the human extracellular part; the chimeric construct restored the antibody-binding completely. Further, we found that in contrast to 8-18C5, MOG-Abs from patients bound preferentially as F(ab')2 rather than Fab. It was previously found that bivalent binding of human IgG1, the prominent isotype of MOG-Abs, requires that its target antigen is displayed at a distance of 13-16 nm. We found that, upon transfection, molecules of MOG did not interact so closely to induce a Förster resonance energy transfer (FRET) signal, indicating that they are more than 6 nm apart. We propose that the intracellular part of MOG holds the monomers apart at a suitable distance for bivalent binding; this

could explain why a cell-based assay is needed to identify MOG-Abs. Our finding that MOG-Abs from most patients require bivalent binding has implications for understanding the pathogenesis of MOG-antibody-associated-disorders. Since bivalently bound antibodies have been reported to only poorly bind C1q, we speculate that the pathogenicity of MOG-Abs is mostly mediated by other mechanisms than complement activation. Therefore, therapeutic inhibition of complement activation should be less efficient in MOG-Ab associated disorders than in patients with Abs to aquaporin-4.

Author affiliations:

1 Institute of Clinical Neuroimmunology, Biomedical Center and University Hospitals, Ludwig-Maximilians-Universität München, 82152 Munich, Germany

2 Physiological Chemistry, Biomedical Center, Ludwig-Maximilians-Universität, 82152 Munich, Germany

3 Department of Neurology, Koc University School of Medicine, 34450 Istanbul, Turkey

4 BioPhysics Core Facility, Biomedical Center, Ludwig-Maximilians-Universität, 82152 Munich, Germany

5 German Center for Neurodegenerative Diseases (DZNE) Munich and Neuroproteomics, School of Medicine, Klinikum rechts der Isar, Technical University of Munich, 81675 Munich, Germany

6 Munich Cluster for Systems Neurology (SyNergy), 81377 Munich, Germany

7 Cellular and Molecular Biophysics, Max Planck Institute of Biochemistry, 82152 Munich, Germany

8 Institute of Lung Biology and Disease (ILBD), Comprehensive Pneumology Center (CPC), Helmholtz Zentrum, 81377 Munich, Germany

Correspondence to: Dr. Edgar Meinl

Institute of Clinical Neuroimmunology, Biomedical Center and University Hospitals, Ludwig-Maximilians-Universität München, Großhaderner Str. 9, 82152 Planegg-Martinsried, Germany

E-mail: ; Edgar.Meinl@med.uni-muenchen.de

Running title: Recognition of MOG by autoantibodies

Keywords: autoimmunity; antigen-recognition; demyelination; neuroinflammation, MOG

Abbreviations:

Abs = antibodies

CBA = cell based assay

CNS = central nervous system

Cyt = cytoplasmic

ED = external domain

ECFP = enhanced cyan fluorescent protein

EGFP = enhanced green fluorescent protein

ELISA = enzyme-linked immunosorbent assay

EYFP= enhanced yellow fluorescent protein

FL = full-length

FRET = Förster resonance energy transfer

IgG = immunoglobulin G

mAb = monoclonal antibody

MOG = myelin oligodendrocyte glycoprotein

MOGAD = MOG-antibody-associated disorders

TMD = transmembrane domain

1. Introduction

The identification of autoantibodies in patients with inflammatory diseases of the central nervous system (CNS) helps to establish a specific diagnosis, which is critical for understanding the pathogenesis and for therapy optimization (Brimberg *et al.*, 2015; Dalmau and Graus, 2018). The recognition of autoantibodies may eventually result in the definition of separate diseases. For example, consensus is now emerging that autoantibodies to myelin oligodendrocyte glycoprotein (MOG) define a separate disease entity, MOG-antibody-associated disorders (MOGAD) (Zamvil

and Slavin, 2015; Jurynczyk *et al.*, 2017; Weber *et al.*, 2018; Reindl and Waters, 2019; Durozard *et al.*, 2020; Mader *et al.*, 2020; Takai *et al.*, 2020).

MOG is displayed on the outer surface of internodal myelin and due to this position it is a target of pathogenic antibodies. While it was demonstrated since the 1980s that autoantibodies to MOG induce demyelination in rodent and primate models of multiple sclerosis (Linington *et al.*, 1988; Genain *et al.*, 1995), the unequivocal identification of MOG-Abs in the blood of patients was achieved much later (O'Connor *et al.*, 2007). MOG-Abs were subsequently connected to acquired demyelinating diseases in children (Brilot *et al.*, 2009; McLaughlin *et al.*, 2009; Pröbstel *et al.*, 2011) and later also to adults with inflammation in the central nervous system (reviewed in (Reindl and Waters, 2019).

One reason for the difficulty to identify patients with MOG-Abs initially was the fundamental difference of MOG-Abs obtained in animal models and MOG-Abs in patients. In animal models, MOG-Abs were readily detected by ELISA (Litzenburger *et al.*, 1998; Pollinger *et al.*, 2009), whereas pathogenic monoclonal antibodies from animals recognized MOG both by ELISA and on the surface of transfected cells (Brehm *et al.*, 1999). To identify patients with MOG-Abs, there is now consensus that an assay using cells transfected with full-length MOG is needed (Tea *et al.*, 2019; Reindl *et al.*, 2020).

MOG is displayed on the membrane. The structure of its extracellular N-terminal part was determined by x-ray crystallography; it forms an Ig-V fold consisting of two antiparallel beta-sheets (Breithaupt *et al.*, 2003; Clements *et al.*, 2003). The prototype rodent anti-MOG mAb 8-18C5 binds to three loops linking the beta-sheets of this N-terminal part with a dominant contribution of His103 and Ser104 in the center of the FG loop (Breithaupt *et al.*, 2003; Breithaupt *et al.*, 2008). MOG-Abs derived from patients are heterogenous and bind to different loops linking the beta-sheets (Mayer *et al.*, 2013; Marti Fernandez *et al.*, 2019; Tea *et al.*, 2019). This N-terminal part of MOG has been recombinantly produced in its correctly folded form and was used for affinity-purification of selected patients' antibodies (Spadaro *et al.*, 2018) as well as detection of MOG-Abs in a few patients (Tea *et al.*, 2019). Thus, the precise conformation of MOG is essential to identify patients with MOG-Abs and correctly folded N-terminal part of MOG alone is not sufficient. The reason for this is currently unknown.

While there is consensus on the extracellular localization and structure of the N-terminal part of MOG, there is dissens about the localization of its C-terminus. Earlier papers indicated that

the C-terminus is intracellular (Kroepfl *et al.*, 1996; della Gaspera *et al.*, 1998), whereas currently Uniprot (27.November.2020) and a recent detailed review with reference to Uniprot (Sinmaz *et al.*, 2016) presented a model where the C-terminus of MOG was localized extracellularly. Thus it is unclear, if this part of MOG contributes to antigen recognition in patients.

The aim of our study was to gain further insights into details of antigen-recognition by MOG-Abs from patients. Specifically, we wanted to understand why a cell-based assay (CBA) is needed to identify patients with MOG-Abs and why the N-terminal external domain of MOG in the correct conformation is not sufficient. To investigate this, we produced the N-terminal part of MOG recombinantly in a correctly folded way and bound it in a site-directed manner to a solid-phase or to lipid-coated beads, then analysed the recognition by MOG-Abs. We revisited the localization of the C-terminal part of MOG with an Ab specific for the C-terminus. We analyzed in detail 14 patients with MOG-Abs using truncated variants of MOG and domain-swapping with parts of the evolutionary distant opossum. We prepared Fab and F(ab')2 fragments to analyze monovalent versus bivalent binding and used Förster resonance energy transfer (FRET) to analyze whether MOG monomers interacted closely with each other.

Our different experimental approaches revealed that most MOG-Abs from patients, but not the prototypic rodent mAb 8-18C5, require the intramembraneous second hydrophobic domain for MOG recognition and bivalent binding is needed. We propose a model in which the second hydrophobic domain of MOG makes two kinks in the membrane around two conserved prolines and is localized within the inner cytosolic membrane leaflet, in agreement with previous reports (Kroepfl *et al.*, 1996; della Gaspera *et al.*, 1998). This structural feature would thereby facilitate lateral clustering and spacing of the extracellular N-terminal part of MOG that allows bivalent binding of autoantibodies. This could explain why a cell-based assay with full-length MOG is needed to identify patients with MOG-Abs. Importantly, he bivalent binding of MOG-Abs has implications for our concepts of pathogenicity of MOG-Abs and therapeutic strategies.

2. Materials and methods

2.1. MOG-variants

Constructs coding for the different variants of the intracellular part of MOG were synthetized from GeneArt (Thermo Fisher Scientific, Waltham, MA, United States) and then cloned into the pEGFP-N1 vector (Clontech Laboratories, Mountain View, CA, United States) fusing the c-terminus to an enhanced green fluorescent protein (EGFP) tag. The ED-MOG (1-155) construct was truncated at glycine 155, thus comprising the whole external domain, the first hydrophobic domain and part of the cytosolic domain (Waters *et al.*, 2015). The whole intracellular cytosolic portion was included in contruct MOG-Cyt by ending the protein at the tyrosine 181. MOG-2TMD includes the whole second hydrophobic domain (until leucine 202) of FL-MOG. The native C-terminus of this construct was substituted with a SGSGGGSGGGSGS linker. The numbering of these constructs is according to (Breithaupt *et al.*, 2003; Mayer *et al.*, 2013) starting with the first coding amino acids (GQF…) and not with the signal peptide.

The MOG sequence of opossum (*Monodelphis domestica*) was taken from the NCBI database and then ordered from Thermo Fisher Scientific GenArt service. The chimeric construct, named Human-Opossum MOG, was designed with human MOG sequence until glycine 155 followed by the cytosolic and second hydrophobic domain from the MOG sequence of the opossum. In this construct, the C-terminus consists of an SGSGGGSGGGSGS linker. Schemes of these constructs are included in **Fig. 4**. Mutants of the N-terminal extracellular part of MOG were described previously (Mayer *et al.*, 2013).

The MOG variants EYFP/CFP-FL-MOG and EYFP/CFP-ED-MOG, with the fluorescent dyes at the N-terminus were also synthetized from GenArt (Thermo Fisher Scientific) and then cloned into the pEGFP-N1 vector, with the consequent removal of the EGFP sequence portion at the C-terminus. The control constructs ECFP, EYFP and the fusion ECFP-EYFP were kindly provided by H. Eibel (Feiburg, Germany) and were described in (Smulski *et al.*, 2017).

2.2. List of Lipids

1,2-Dioleoyl-*sn*-glycero-3-phosphocholine (dioleoylphosphatidylcholine; DOPC) (Avanti Polar Lipids, Alabaster, AL, United States)

1,2-Dioleoyl-*sn*-glycero-3-phosphoethanolamine-*N*-(cap biotinyl) (18:1 Biotinyl Cap PE) (Avanti Polar Lipids)

1,2-Dioleoyl-*sn*-glycero-3-phosphoethanolamine labeled with Atto 488 (Atto488 DOPE) (Sigma Aldrich, St. Louis, MO, United States)

2.3. Recombinant production of correctly folded extracellular part of MOG

The extracellular part of human MOG (amino acids 1-125) with an Avi-tag allowing enzymatic biotinylation and a His-tag was recombinantly produced using the HEK-EBNA cells and the pTT5 vector (Perera *et al.*, 2013). MOG-1-125 was secreted in serum-free supernatant, purified via its His-tag and its correct folding was assessed using circular dichroism as described (Spadaro *et al.*, 2018; Marti Fernandez *et al.*, 2019). The glycan of this MOG-1-125 has a similar size as the glycan of FL-MOG on transfected cells and its glycoforms have been described (Marti Fernandez *et al.*, 2019). This material was used for ELISA, for binding to lipid-coated beads and for affinity-purification of MOG-Abs.

2.4. Affinity purification of MOG-Abs from patients

The autoantibodies against MOG present in the plasma of patient #7 were affinity-purified using correctly folded extracellular part of MOG bound to streptavidin columns as previously described in (Spadaro *et al.*, 2018).

2.5. Enzyme-linked immunosorbent assays (ELISAs) detecting MOG-Abs and recombinant monoclonal antibodies

We applied two ELISAs. First, MOG-1-125 was bound to MaxiSorp (Thermofischer, Waltham, MA, United States) and compared with BSA-coated wells. Second, MOG-1-125 was biotinylated at its Avi-tag with the BirA biotin ligase Kit (Avidity, Aurora, CO, United States) and then bound to streptavidin plates and compared to streptavidin wells, since we saw that adding BSA to streptavidin-coated plates resulted in essentially the same results as using streptavidin-coated plates alone. The ELISA assays were validated by a recombinant mAb against MOG (r8-18C5) and a

control mAb against Borrelia (HK-3) (**Suppl. Fig. 1**), both having a human IgG1-Fc part (Brändle *et al.*, 2016; Spadaro *et al.*, 2018). Serum was diluted 1:200 and binding of antibodies was detected with an anti-human IgG conjugated to horseradish peroxidase (Jackson ImmunoResearch, West Grove, PA, United States).

2.6. Localization of the C-terminus of MOG

Two different cell lines were used for this part of our study: HeLa cells transiently transfected with FL-MOG or ED-MOG, each fused to EYFP at the N-terminus and the TE-671 cell line (rhabdomyosarcoma cells) stably transfected with FL-MOG without any fluorescent tag (Pröbstel *et al.*, 2011). HeLa cells were fixed with 2% PFA and permeabilized with Intracellular Staining Perm Wash Buffer (BioLegend, San Diego, CA, United States). TE671 cells were fixed and permeabilized with Cyto-Fast Fix/Perm Buffer Set (BioLegend, United States). To detect MOG, the r8-18C5, which binds to the FG-loop in the extracellular part of MOG (Breithaupt *et al.*, 2003) and the commercially available Ab28766 (Abcam, Cambridge, UK, England), which binds the last 12 amino acids of MOG at the C-terminus (AGQFLEELRNPF), were applied.

2.7. Lipid coating of silica beads and binding of MOG

Silica beads (SiO_2-R-6.0) of 6.16 µm in diameter (microParticles, Berlin, Germany) were coated with a lipid bilayer as follows. First, a mixture of DOPC, Biotinyl CAP PE, Atto488 DOPE in chloroform was prepared at a 98:1:0.03 molar ratio inside a glass vial. A lipid film was formed on the walls of the vial by gently evaporating the solvent with a nitrogen stream and by subsequently drying under vacuum for 20 minutes. The lipid film was then rehydrated with 200 µl of PBS (Gibco, Thermo Scientific, Waltham, MA, United States), 100 µl beads solution (at 6 mg/ml of concentration) and resuspended via vortexing until the solution became turbid. Following this, The beads were coated with the lipids through 30 minutes of sonication in a bath sonicator until the solution cleared.

The extent of the coating was determined in the first place by checking the green fluorescent signal of Atto488 DOPE on the beads via confocal microscopy imaging with an LSM 780 microscope using a 40x/1.2 W C-Apochromat objective (Carl Zeiss AG, Oberkochen, Germany).

We bound the biotinylated MOG-1-125 with neutravidin (Invitrogen, Carlsbad, CA, United States) to the Biotinyl CAP PE. We showed that it was displayed on the coated beads surface by detecting it with the r8-18C5 and Alexa Fluor 647 goat anti-human IgG (H+L) antibody (Invitrogen) as the secondary antibody. The fluorescent signal was detected via confocal microscope imaging and via flow cytometry with FACSverse (BD Biosciences, San Jose, CA, United States).

2.8. Quantification of anti-MOG reactivity on lipid coated beads

We quantified the anti-MOG reactivity of several sera and of the humanized r8-18C5 via flow cytometry (BD Bioscences, San Jose, CA, United States). We gated on all the fluorescent beads with an Atto488 signal >100 and then we calculated their MFI in the APC channel. The MFI ratio was obtained by dividing the MFI of the beads bound to biotinylated MOG-1-125 incubated with sera or r8-18C5 by the MFI of the fluorescent beads not bound by biotinylated-MOG-1-125 incubated with sera or r8-18C5. All the signals were quantified by using FlowJo software (LLC, BD life sciences).

To test for recognition by sera with MOG-Abs, the beads were resuspended in 400 µl of FACS buffer, then 100 µl were incubated with serum diluted 1:50 in FACS Buffer. Binding of antibodies in serum was detected with Alexa Fluor 647 goat anti-human IgG (H+L) antibody (Invitrogen). The fluorescent signal was detected via flow cytometry with FACSverse (BD Biosciensces).

2.9. Cell based assay (CBA) to quantify recognition of MOG variants

The reactivity of the patients' antibody to the different MOG variants was detected in a live-cell-based assay as previously described (Mayer *et al.*, 2013; Spadaro *et al.*, 2018) with FACSverse flowcytometer (BD Biosciences). HeLa cells were transiently transfected via Lipofectamine 2000 (Thermo Fisher Scientific, Waltham, MA) with the different MOG constructs or with EGFP alone (control). To detect the binding of antibodies in serum (diluted 1:50) to the transfected cells, we used biotin-SP-conjugated goat anti-human IgG (1:500 diluted) (Jackson ImmunoResearch, West Grove, PA, United States) as secondary antibody. Subsequently, Alexa

Fluor 647-conjugated streptavidin was added (1:2000). Dead cells were excluded from the experiment with Propidium Iodide staining (1:2000 in PBS).

All of our MOG-constructs were expressed as fusion proteins with EGFP allowing the direct quantification of MOG expression via the EGFP signal. We noted that the different MOG constructs were expressed to a different intensity (**Suppl. Fig. 2**). This was taken into consideration and the gating for the default quantification was set to EGFP 100-500, because all MOG-constructs showed a decent expression with this gating criteria (**Suppl. Fig. 2A**). Thus, the anti-MOG reactivity was quantified by gating the cells with EGFP-signal between 100-500 and determining their mean fluorescence intensity (MFI) in the APC channel. We subsequently calculated the MFI ratio of cells expressing MOG-EGFP and cells expressing EGFP alone. All the signals were quantified by using FlowJo software (LLC, BD life sciences, Ashland, OR, United States).

2.10. Consideration of different expression intensities of the applied MOG-mutants

We displayed all MOG-variants as EGFP-fusion proteins as this allowed a precise quantification of MOG expression. We noted that the six MOG mutants differed in their intensity of expression. MOG-2TMD and human-opossum-MOG showed the highest expression. (**Suppl. Fig. 2**). All MOG-constructs yielded a decent expression within the EGFP gate of 100-500 (**Suppl. Fig. 2**). Therefore this EGFP gate of 100-500 was our default setting for quantification of the reactivity towards the different constructs.

We show the reactivity towards each MOG-construct for all analyzed patients using two different gatings, EGFP>100 and EGFP 100-500 (**Suppl. Fig. 3A and 3B**). While in most instances the graphs in **Suppl. Fig. 3A and 3B** look similar, these two presentations provide complementary information in special instances. For example, for patient #22 the response to ED-MOG appears higher than FL-MOG in **Suppl. Fig. 3B**, but when considering the EGFP gates of 100-500, it becomes clear that this patient recognized ED-MOG and FL-MOG similarly. Thus, the apparently higher response to ED-MOG of patient #22 was only due to the higher percentage of cells expressing higher levels of ED-MOG than FL-MOG. This applies also to other patients like #14, #38, #41, #42 and #16, whose reactivity to ED-MOG would be missed completely with the gate setting of EGFP 100-500.

2.11. Förster resonance energy transfer (FRET) experiment to assess MOG dimerization

We performed our FRET experiments essentially as described in (Smulski *et al.*, 2017). Briefly, we transiently transfected HEK293T cells with the ECFP and EYFP MOG fusion constructs described in 2.3. The cells were subsequently analyzed 16-20 hours post-transfection. All FRET experiments were performed with a LSR Fortessa (BD Biosciences). The EYFP signal was detected using the 488 nm laser with a 540/30 filter, ECFP signal was detected using the 405 nm laser with a 450/40 filter and FRET signal was recorded using the 405 nm laser with a 540/30 filter. We defined the positive FRET gating by using cells expressing an ECFP–EYFP fusion protein as positive control. To define the FRET negative gating, cells were co-transfected with ECFP and EYFP .

2.12. Production of Fab and F(ab')2 from patients' plasma and analysis of their MOG recognition

IgG was purified from plasma with Protein G HP SpinTrap columns (GE Healthcare Life Sciences, Chicago, IL). Subsequently, the IgG concentration was measured with a Human IgG ELISA kit (Mabtech, Nacka Strand, Sweden). The IgG concentration range of the purified plasma samples spanned between 2.5 and 7 mg/ml. Fab and F(ab')2 fragments were then generated with the Pierce Fab/F(ab')2Preparation Kit (Thermo Fisher Scientific, Waltham, MA, United States). The Fab fragments were further purified by Size Exclusion Chromatography to separate them from the pool of undigested IgGs using a SuperdexIncrease 200 10/-300 GL column (GE Healthcare Life Sciences, Chicago, IL, United States). Peak fractions were analyzed by SDS-PAGE and Coomassie staining, elution fractions containing only digested Fabs were finally pooled and used for downstream assays.

To detect binding of the Fab and F(ab')2 fragments to MOG, a different secondary antibody from the one used for detection of anti-MOG in serum had to be used, since the secondary Ab used for evaluating serum includes reactivity to the Fc-part of the IgG, which is no longer present after the Fab and F(ab')2 preparation. We used an Alexa Fluor 647 mouse anti-human Ig light chain κ antibody together with an Alexa Fluor 647 mouse anti-human Ig light chain λ antibody, both 1:100 diluted (BioLegend, San Diego, CA, United States). The fluorescent signal was further amplified

by the use of a rat anti-mouse IgG Alexa Fluor 647 antibody diluted 1:500 (Jackson ImmunoResearch, West Grove, PA, United States). r8-18C5 was produced recombinantly with the human heavy chain from the J-element onwards, but a murine light chain (Brändle *et al.*, 2016; Spadaro *et al.*, 2018). Therefore, this Ab and its Fab and F(ab')2 were detected with an anti-human IgG + IgA + IgM (H+L) (Jackson ImmunoResearch, West Grove, PA, United States) as secondary Ab.

2.13. Statistics

For statistical analysis, we used the GraphPad Prism7 programm (GraphPad software, San Diego, CA, United States). For the quantification of the reactivity of the 14 patients with MOG-Abs towards the six different MOG variants we set the reactivity towards FL-MOG to 100% and normalized the reactivity towards the other constructs . We then used a one-way ANOVA Tukey´s multiple test comparison to quantify the significance of the recognition of the different constructs.

2.14. Patients and control subjects

For the comparative analysis of MOG-recognition by ELISA versus cell-based assay we used serum samples from 18 patients with MOGAD (average age: 38 years old, 10 females, 9 males). To set the threshold, we analyzed 13 healthy donors. To set the threshold for our CBA we had included over the years 87 healthy controls (average age: 35 years old, 53 females, 34 males). For the analysis of the recognition of MOG-variants, we used serum samples and plasma samples of 14 patients with MOGAD (average age: 39 years old, 6 females, 8 males), who showed a strong MOG-reactivity in the CBA including 12 patients from the above comparison (indicated with filled circles in **Fig. 1**). For comparsion, one patient who scored negative in the cell-based assay and the ELISA was included throughout (designated as C). Patients with MOG-Abs, #5, #7, #10, #14, #16 and #17 were described in (Spadaro *et al.*, 2018); and #22, #23, #24, #38, #39, #41, #42, #43 in (Winklmeier *et al.*, 2019). Informed consent was obtained from each donor according the Declaration of Helsinki and the ethical committee of the medical faculty of the LMU approved the study.

2.15. Data availability

The data presented in the manuscript are available from the corresponding author on request.

3. Results

3.1. The extracellular part of MOG displayed site-directed on an ELISA plate allows detection of MOG antibodies only in few patients

The epitopes of MOG recognized by autoantibodies from patients are located in the loops that link the β-sheets of the extracellular part of MOG (Mayer *et al.*, 2013; Tea *et al.*, 2019). We produced this extracellular part in a correctly folded form and confirmed the beta-sheet conformation by circular dichroism (Spadaro *et al.*, 2018; Marti Fernandez *et al.*, 2019). We used this part of MOG for two ELISA variants. In one, MOG-1-125 was bound to typical MaxiSorp plates and in the other MOG-1-125 was enzymatically biotinylated at the Avi-tag of its C-terminus and bound in a site-directed manner to streptavidin plates. Both ELISAs were validated with r8-18C5 (**Suppl. Fig. 1**). We analysed 18 patients with MOG-Abs and compared the anti-MOG-reactivity obtained by CBA using full-length MOG with the recognition of MOG by the two ELISA variants (**Fig. 1**). The MaxiSorp ELISA detected MOG-Abs in 4/18 patients, while the streptavidin-biotinylated MOG-ELISA detect 9/18 patients with MOG-Abs. Thus, an ELISA using site-directed binding of MOG-1-125 is superior to a random binding of MOG-1-125. However, even this improved ELISA did not detect half of the patients who scored positive in a CBA with MOG-transfected cells.

3.2. The C-terminus of MOG is intracellular

Since MOG-1–125 used in the ELISA assay had a sensitivity to detect MOG-Abs in patients' sera, we specifically revisited whether the C-terminus of MOG (from amino acid 203 to 218) is intracellular or extracellular. We used ab28766, specific for the last 12 amino acids of MOG (**Fig. 2A**), and the mAb r8-18C5 that binds to a defined loop on the extracellular part of MOG

around amino acid 103 (Breithaupt *et al.*, 2003) (**Fig. 2A**). Both antibodies were tested on HeLa cells transiently transfected with FL-MOG or ED-MOG tagged at the N-terminus with EYFP to ensure that the fluorescent tag does not interfere with the binding of the Ab to the C-terminus. Additionally, TE-671 cells (rhabdomyosarcoma cells) stably transfected with FL-MOG without any tag (Pröbstel *et al.*, 2011) were used (**Fig. 2B-I**).

The mAb r8-18C5 bound to FL-MOG and ED-MOG in HeLa cells as well as the FL-MOG in TE-671 cells, in both living and fixed conditions. **(Fig. 2B, 2C, 2F, 2G**). In contrast, the ab28766, failed to detect MOG in both cell lines when living cells were analyzed (**Fig. 2D and 2H**). However, once the cells (HeLa and TE671) were fixed and permeabilized, the ab28766 bound to EYFP-FL-MOG in HeLa cells and also to the FL-MOG stably expressed on the TE-671 cells (**Fig. 2E and 2I**). As a further control for the specificity of the applied antibodies, we used HeLa cells transfected with ED-MOG (lacking the C-terminus). These cells were not recognized by the ab28766, neither in the viable nor fixed and permeabilized conditions (**Fig. 2D and 2E**). We conclude that the C-terminus of the MOG protein is intracellular. Thus, the patient samples that recognized FL-MOG in live CBAs had bound to the N-terminal extracellular part of MOG.

3.3. Displaying MOG-1-125 in a fluid lipidic environment does not improve antibody detection

Having seen the drastic difference between MOG-1-125 bound to an ELISA plate and FL-MOG displayed on transfected cells, we tested the effect of embedding of MOG in a lipid environment on Ab recognition. Thus, we explored the impact of a fluid lipidic environment on the detection of ED-MOG, by designing a new assay.

We coated silica beads of dimensions similar to cells (6 µm of diameter) with a lipid mixture that would mimic the lipid bilayer that forms the cell membrane (**Fig. 3A**). To monitor the lipid-coating of the beads, the mixture contained fluorescently labelled lipids with Atto488 and biotinylated lipids for a neutravidin bridge to attach biotinylated MOG-1-125. The biotinylated MOG-1-125 is correctly folded as assessed by circular dichroism (Spadaro *et al.*, 2018; Marti Fernandez *et al.*, 2019) and is expected to move freely along the lipid bilayer when linked to the biotinylated lipid via neutravidin (Ramm *et al.*, 2018). MOG-1-125 bound to lipid-coated beads, could be detected by r8-18C5 (**Fig. 3A, 3C and 3D**). However, the intensity of the binding was

lower in comparison to FL-MOG or ED-MOG expressed in transiently transfected cells (**Fig. 3D**). We incubated these beads with sera of five patients (#5, #14, #16, #17 and #22) (**Fig. 3E**). Three of these patients (#5, #17 and #22) weakly recognized MOG displayed by these beads. Those three patients were also detected by the site directed ELISA (**Fig. 1B**). Nevertheless, the MOG-1-125 in the site directed ELISA was also capable of binding the antibodies of patient #16. Therefore, we conclude that the embedding of MOG-1-125 in a fluid lipidic environment does not improve the antibody detection.

3.4. The second hydrophobic domain of MOG is crucial for MOG recognition by most patients

We tested sera from 14 patients with MOG-Abs for recognition of HeLa cells transfected with FL-MOG or ED-MOG. For comparison, we also show the reactivity of one MOG negative patient (#C) to all of our mutants (**Fig. 4 and 5, Suppl. Fig. 3**). All of the 14 MOG+ patients recognized FL-MOG much better than ED-MOG ($p<0.0001$) (**Fig. 5B**). **Fig. 4** shows details of representative patients. **Fig. 5 and Suppl. Fig. 3** show the summary of all analysed patients and related statistics. Overall, only five patients out of the 14 MOG+ (36%) were detected by cells transfected with ED-MOG (**Fig. 5A and Suppl. Fig. 3A**). Thus, not only in the ELISA assay, but even in the CBA was ED-MOG poorly recognized by most patients, deeming it insufficient to detect MOG-Abs. The detailled recognition of epitopes of MOG was determined for 12 of the 14 patients and they recognized different epitopes as seen with point-mutations of the loops linking the beta-sheets of the N-terminal part of MOG (**Suppl. Fig. 5**). Thus, the strong recognition of FL-MOG as compared to ED-MOG is not related to certain epitopes on the extracellular part of MOG, but is rather a general feature of MOG-Abs from patients.

We went on to narrow-down the intracellular domains of MOG, which increase the antibody detection of the extracellular domain. Hence, we designed two MOG variants. The first one is composed of the extracellular part, the first transmembrane domain and the cytoplasmic part until the second hydrophobic domain (Tyr181); named MOG-Cyt (**Fig. 4**). Secondly, we cloned a longer variant of MOG that included the second hydrophobic domain (until leucine 202), called MOG-2TMD (**Fig. 4**). These variants were tested for recognition by autoantibodies from our 14 patients (**Fig. 5 and Suppl. Fig. 3**).

The raw data in the dot-plots already indicate that the three representative patients #5, #7 and #14 strongly recognized MOG-2TMD, but only weakly MOG-Cyt (**Fig. 4**). Considering all patients, MOG-Cyt was far less recognized than MOG-2TMD or FL-MOG ($p<0.0001$) (**Fig. 5; Suppl. Fig. 3A**). In particular, the reactivity towards MOG-Cyt dropped in 13/14 patients even below 20% compared to FL-MOG (**Fig. 5B**). Together, this part of our analysis identified the second hydrophobic domain of MOG as the crucial non-extracellular part of MOG to enhance recognition of its extracellular part by autoantibodies from patients.

To further elaborate the impact of the secon hydrophobic part of MOG for antigen-recognition, we analysed the recognition of full-length MOG from the evolutionary distant opossum (*Monodelphis domestica*) and of a chimeric construct composed of the extracellular and first hydrophobic domain of human MOG fused to the cytoplasmic and second hydrophobic domain from opossum (**Fig. 4**). The group of patients with MOG-Abs recognized opossum MOG weaker than human FL-MOG ($p<0.0001$) (**Fig. 5A**). We also observed a heterogeneous recognition of opossum-MOG by patients: compared to human FL-MOG, out of 14 MOG+ patients, seven showed a weak cross-reactivity to opossum-MOG (recognition below 20%). Two patients recognized it similarly (#39 and #10), and another two recognized the opossum-MOG even better than the human MOG (#7 and #22) (**Fig. 4 and Suppl. Fig. 3**). Strikingly, the human-opossum construct was detected by all 14 MOG+ patients. Of note, the four patients (#14, #38, #41 and #42) who did not show cross reactivity to opossum-MOG had also detected the human-opossum construct (**Fig. 5, Suppl. Fig. 3A**). Human-opossum MOG was better recognized than ED-MOG by all 14 patients ($p<0.0001$) (**Suppl. Fig. 3A**). Thus, the intracellular part of opossum-MOG greatly enhances recognition of the extracellular part of human MOG. In contrast to patients with MOG-Abs, the mAb r8-18C5 recognized all these MOG variants similarly, as elaborated in a dose-response (**Suppl. Fig. 4**).

3.5. MOG-Abs affinity-purified with the extracellular part of MOG still recognize preferentially full-length MOG

We have affinity-purified MOG-Abs using MOG-1-125 from patient #7, who showed a typical and strong recognition of FL-MOG while a weak recognition of ED-MOG (**Fig. 4**). Remarkably, not only the serum antibodies, but also the MOG-Abs affinity-purified with the

recombinantly produced MOG-1-125 recognized FL-MOG much better than ED-MOG in transfected cells. (**Suppl. Fig. 6A**). We noted that this type of affinity-purification does not extract all MOG-Abs, a substantial amount was still present in the flow-through. We compared the affinity-purified antibodies with the starting material (plasma) and the flow-through with respect to recognition of mutated variants of the extracellular part of MOG, which are known to identify MOG epitopes (Mayer *et al.*, 2013). This showed that the MOG-Abs that were affinity-purified with the ED-MOG recognized the same epitopes on the extracellular part of MOG as the crude plasma and as the antibodies in the flow-through (**Suppl. Fig. 6B**). Together, these experiments indicate that MOG-Abs of the same antigenic immunoreactivity within one patient strongly recognize FL-MOG and weakly ED-MOG.

3.6. Bivalent recognition of MOG required by antibodies from patients

We analysed the importance of bivalent binding for the differential recognition of FL-MOG and ED-MOG. To this end, we generated with pepsin and papain digestion Fab and F(ab')2 fragments of the r8-18C5 as well as IgGs of four patients (#14, #16, #17 and #22). We picked a highly reactive MOG patient (#14), one medium reactive (#16), one patient (#17), whose antibodies were also detected in the ELISA assay (**Fig. 1**), and patient #22, whose antibodies were also detected by ELISA and bound strongly to ED-MOG and FL-MOG (**Fig. 4**). F(ab')2 fragments were obtained by pepsin digestion; F(ab) fragments were obtained by digestion with papain and subsequent size exclusion chromatography (SEC) to separate the undigested pool of antibodies from the Fab fragments (**Fig. 6A**).

We compared the reactivities of Fab and F(ab')2 fragments on cells transfected with FL-MOG or ED-MOG. The F(ab')2 fragments from the four patients behaved in the same manner as the purified IgGs (**Fig. 6B**). The Fab preparations of all four analyzed patients showed little or no recognition of either FL-MOG or ED-MOG (**Fig. 6B**). In contrast, the Fab from r8-18C5 clearly bound to both FL-MOG and ED-MOG. A dose response of r8-18C5 and its Fab and F(ab')2 fragments demonstrated that the recognition of Fab is slightly weaker than of F(ab')2, but Fab and F(ab')2 of this mAb did not differentiate between FL-MOG and ED-MOG (**Suppl. Fig. 7**). Together, this part illustrates that MOG-Abs from patients, but not the mAb r8-18C5, strictly

require bivalent recognition to bind to MOG. The need for bivalent binding and the importance of the second hydrophobic together are presented in our model in **Fig. 7**.

3.7. FRET does not show dimerization of ED-MOG or FL-MOG

We investigated whether FL-MOG or ED-MOG formed dimers detected by FRET. To this end,we co-transfected HEK-293T cells with ECFP-FL-MOG and EYFP-FL-MOG or with ECFP-ED-MOG and EYFP-ED-MOG. These experiments revealed that neither FL-MOG, nor ED-MOG came so close to each other that this would result in a FRET signal. In contrast, the positive control, fusion protein ECFP-EYFP yielded a strong FRET signal (**Suppl. Fig. 8**).

4. Discussion

We report that the second hydrophobic domain of MOG enhances recognition of its N-terminal extracellular part in most patients and propose that this is the reason why a cell-based assay with FL-MOG is the gold-standard to identify patients with MOG-Abs. Most MOG-Abs from patients recognize loops that link the beta-sheets of the IgV-like fold of the extracellular N-terminal part of MOG (Mayer *et al.*, 2013). This part of MOG (MOG-1-125) can be produced in a conformationally correctly folded way (Spadaro *et al.*, 2018; Marti Fernandez *et al.*, 2019; Tea *et al.*, 2019), but this is not sufficient to identify MOG-Abs positive patients. This was seen in a recent study, where MOG was bound in a random way to an ELISA plate (Tea *et al.*, 2019). Our study confirms this and shows that a site-directed display of MOG on the ELISA is superior, but still insufficient to identify all patients with MOG-Abs.

We found that MOG-1-125 embedded in a fluidic lipid environment is recognized by the anti-MOG mAb r8-18C5 and weakly by patients, but far less efficient than MOG in transfected cells. Therefore we worked out details of MOG-recognition in transfected cells and found that most patients recognized FL-MOG much better than ED-MOG. This is in accordance with a previous report (Waters *et al.*, 2015). We went on to dissect the contribution of the intracellular part of MOG for the enhanced recognition of FL-MOG with different truncated variants of MOG and this revealed that the second hydrophobic domain of MOG is crucial for the detection of MOG by patients with MOG-Abs.

We continued to analyze whether this enhanced recognition of MOG by the intracellular part is based on a specific sequence of MOG or rather based on the overall structure of MOG. While wrapped myelin is found in vertebrates, MOG is found only in mammals. We expressed MOG from opossum, the evolutionary most distant animal from whom a MOG-sequence was available in the NCBI database. Most patients did not or only weakly recognize MOG from opossum. This was expected, since many patients do not even show cross-reactivity to rodent MOG (Mayer *et al.*, 2013; Peschl *et al.*, 2017; Spadaro *et al.*, 2018). Importantly, when we constructed a chimeric MOG, with the N-terminal ED part from human MOG and the C-terminal part from opossum MOG, this MOG-construct was recognized as strongly as the full-length human MOG. We observed this enhanced recognition of MOG by the second transmembranous domain of MOG in patients who recognize different eptiopes on the extracellular part of MOG. This argues that the second hydrophobic domain does not induce the exposure of a specific epitope, but induces an overall structure of MOG that is better recognized by autoantibodies.

We tested whether the enormous difference in recognition of ED-MOG versus FL-MOG could be attributed at least partially to an extracellular display of the C-terminal part of MOG. All of our experiments using both transiently and stably transfected cells, came to the same conclusion, namely that the C-terminus is intracellular. Our observation is in line with earlier reports (Kroepfl *et al.*, 1996; della Gaspera *et al.*, 1998), but at variance with the current prediction of Uniprot (27.November.2020), and a model presented in a recent review with reference to Uniprot (Sinmaz *et al.*, 2016). Our model in **Fig. 7** includes the specific amino acid composition of the second hydrophobic domain of MOG and their adjacent amino acids: the second hydrophobic domain has two prolines. A proline might indicate a kink in the α-helix (von Heijne, 1991; Nilsson *et al.*, 1998) A similar monotopic domain displaying an analogous structure with two hydrophobic helices and a proline in the middle (helix-break-helix) is also seen for caveolin (Aoki *et al.*, 2010) and for the transmembrane protein PEN-2, a subunit of the Alzheimer's disease- and Notch-signaling-related protease γ-secretase (Pittock *et al.*, 2019; Zhou *et al.*, 2019). Also, the three positively charged amino acids next to the hydrophobic domain that were expected to bind to negatively charged lipids intracellularly and the cysteine at the end of the hydrophobic domain that might be palmitoylated (Smotrys and Linder, 2004) are linked to the intracellular localization of the C-terminus of MOG. These four amino acids are also conserved from opossum to human (**Suppl. Fig. 9**). Further, we found that all patients with MOG-Abs recognized the mutant MOG-2TMD, which does not include

the C-terminus, at least as strongly as FL-MOG. Together, this part of our study establishes that the C-terminus of MOG is intracellular and in contrast to the second hydrophobic domain, not involved in binding of patient antibodies to FL-MOG.

To offer further insight into details of MOG-recognition, we analyzed whether FL-MOG or ED-MOG form close dimers detectable by FRET and we analyzed monovalent versus bivalent binding to FL-MOG and ED-MOG. We found that neither ED-MOG nor FL-MOG give a FRET signal. The intensity of a FRET signal is inversely proportional to the sixth power of the inter-dye distance and this energy transfer process can serve as a spectroscopic ruler in the 1-6 nm range (Stryer and Haugland, 1967). Thus, our FRET experiments show that ED-MOG or FL-MOG are further apart from each other than 6 nm. To allow bivalent binding of IgG1 (the typical isotype of MOG-Abs), the target antigen has to be at a relatively strict distance of about 13-16 nm as recently corroborated with DNA origami technology (Shaw *et al.*, 2019). In a crystallographic paper, ED-MOG was reported to form a head-to-tail dimer (Clements *et al.*, 2003); in the same paper, MOG extracted from myelin appeared by Western-blot largely monomeric, but also a minor proportion of dimeric forms of MOG were observed indicating that MOG may form dimers under special crystallization conditions and also in myelin. Our FRET experiments do not exclude dimer formation of MOG under certain situations, but show that under our experimental conditions, cells transfected with MOG for a CBA, MOG does not associate closer than 6 nm. In accordance with our FRET data, MOG from transfected cells appeared as a monomer when Western blots of transfected cells were performed (Mayer *et al.*, 2013; Marti Fernandez *et al.*, 2019).

We found that MOG-Abs from four patients bound strongly in the form of F(ab')2, but poorly or not at all as Fab, indicating that these MOG-antibodies largely require bivalent binding to be detected. The dependence on bivalent binding is most likely due to concentration and affinity. In particular, it argues that the affinity of human MOG-Abs is lower than of 8-18C5 and therefore a gain of avidity due to bivalent binding is needed for a clear binding to MOG. Also, in vitro-translated extracellular part of MOG constructed to form tetramers is recognized by MOG-Abs from patients (O'Connor *et al.*, 2007). We speculate that FL-MOG is better recognized than ED-MOG, because the intracellular part of MOG induces a clustering of MOG with a spacing of the extracellular part of MOG that allows bivalent Ab-binding, illustrated in **Fig. 7**. The second hydrophobic domain could hold the monomers apart at a suitable distance that would facilitate the bivalent binding of the MOG-Abs, presumably involving lipid rafts (Kim and Pfeiffer, 1999). This

model is in accordance with previous studies that showed that crosslinking of MOG-Abs induces signaling (Marta *et al.*, 2005) and lateral diffusion of transfected MOG in the membrane is anomalous and slowed down (Gielen *et al.*, 2005; Gielen *et al.*, 2008). We are aware that our model in **Fig. 7** might not be the only possible explanation for the enhanced recognition and bivalent binding of MOG-Abs when the second hydrophobic domain is present. It could also be that the second hydrophobic domain creates an empty space around the MOG molecules which favors the binding of MOG-Abs.

We assume that the few patients whose MOG-Abs give some signal using MOG-1-125 bound to an ELISA plate or to ED-MOG in transfected cells, have such a strong affinity that allows monovalent binding. This view is also strengthened by features of the mAb r8-18C5, which has a strong affinity to MOG, binds also as Fab to MOG, recognizes ED-MOG and FL-MOG in transfected cells similarly and also MOG by ELISA. Together, we show that MOG-Abs from most patients require bivalent binding to be detected. We propose that bivalent binding is facilitated with cells transfected with FL-MOG (or MOG-2TMD), but not when ED-MOG is transfected or when MOG-1-125 is bound to an ELISA plate.

Patients with antibodies to MOG or AQP4 show clinically overlapping features, but consensus is emerging that anti-MOG and anti-AQP4 constitute separate diseases (Zamvil and Slavin, 2015; Fujihara, 2019; Mader *et al.*, 2020). While this study indicates that MOG-Abs from most patients require bivalent binding for antigen-recognition, autoantibodies to AQP4 have been reported to bind also as monomer (Crane *et al.*, 2011). Monovalent binding of IgG provides a more efficient platform for C1q binding and complement activation than bivalent binding (Diebolder *et al.*, 2014; Soltys *et al.*, 2019). Previous work has shown that complement-mediated activation by MOG-Abs in vitro was restricted to high titre positive patients (Mader *et al.*, 2011). Thus, MOG-Abs may activate complement, but they do this far less efficient than by AQP4-Abs. This view is supported by histopathological examinations: although C9neo deposition can be observed in patients with MOG-Abs (Spadaro *et al.*, 2015; Jarius *et al.*, 2016; Kortvelyessy *et al.*, 2017; Hoftberger *et al.*, 2020) or after transfer of their MOG-Abs (Spadaro *et al.*, 2018), it is far less pronounced than in patients with antibodies to AQP4 (Lucchinetti *et al.*, 2002; Bradl *et al.*, 2009; Takai *et al.*, 2020). In particular, patients with AQP4-Abs have large perivascular complement deposition that is missing in MOGAD (Weber *et al.*, 2018; Mader *et al.*, 2020).

While IgGs from patients with AQP4-Abs readily induce disease upon transfer (Bradl *et al.*, 2009), this has been difficult to achieve with IgG preparations from MOG-Abs positive patients and it took affinity purification of antibodies from selected patients to achieve this (Spadaro *et al.*, 2018). These affinity-purified Abs that transfer disease also recognize MOG by ELISA as shown here. Recognition of MOG by ELISA by a few patients was interpreted as an indicator of high affinity (Tea *et al.*, 2019), suggesting that these patients' antibodies might bind monovalently. Along this line, only a single patient with high-titre antibodies to MOG was able to induce complement-dependent tissue injury in an ex vivo organotypic brain slice model (Peschl *et al.*, 2017) and no complement-dependent changes were observed upon intracerebral injection of pooled IgG from MOG positive patients (Saadoun *et al.*, 2014). Complement-independent pathomechanisms of MOG-Abs include also cytoskeletal alterations (Dale *et al.*, 2014) and antibody-mediated cellular cytotoxicity (Brilot *et al.*, 2009).

The observations from pathology and our finding that MOG-Abs largely bind bivalently have therapeutic implications. This suggests that the anti-complement therapy with eculizumab, which is very successful in patients with anti-AQP4 (Pittock *et al.*, 2019) might be less effective in patients with MOG-Abs. Autoantibodies may induce pathology by multiple mechanisms other than complement activation, including endocytosis and FcR activation (Ludwig *et al.*, 2017; Dalmau and Graus, 2018). In animal models of hemolytic anemia, low-affinity bivalently binding autoantibodies were highly pathogenic (Fossati-Jimack *et al.*, 1999). MOG-Abs affinity-purified from patients were pathogenic by enhancing activation of cognate T cells (Spadaro *et al.*, 2018), presumably by accumulating in CNS-resident phagocytes (Flach *et al.*, 2016) and enhancing T cell activation via FcR-dependent opsonization of MOG (Kinzel *et al.*, 2016).

Together, we report that MOG-Abs from most patients require the intracellular part of MOG to recognize its extracellular part and show a bivalent binding to MOG. These features of human MOG-Abs explain why a cell-based assay with FL-MOG is the gold-standard to identify such patients and have implications for our concept about pathogenicity of human MOG-Abs.

5. Acknowledgements

We are grateful to Heike Rübsamen for technical assistance and Prof. Hartmut Wekerle for the continuous support. We are grateful to Prof. Hermann Eibel for kindly providing the FRET control constructs. We thank Samantha Ho together with Drs Naoto Kawakami and Klaus Dornmair for comments on the manuscript. FRET experiments were supported by Dr. L. Richter, Core Facility Flow Cytometry at the Biomedical Center, LMU Munich.

6. Funding

This study was funded by the DFG (SFB TR128) and under Germany's Excellence Strategy within the framework of the Munich Cluster for Systems Neurology (EXC 2145 SyNergy– ID 390857198), the Werner Reichenberger Stiftung and the Verein zur Therapieforschung für MS-Kranke.

7. Competing interests

The authors declare no competing interests.

8. Figure legends

Fig. 1: **Comparison of MOG-reactivity by ELISA and cell-based assay (CBA).** The anti-MOG-reactivity of 18 patients with MOG-Abs was determined by CBA using FL-MOG and by ELISA. CBA was performed as described (Spadaro *et al.*, 2018) and the anti-MOG reactivity is shown as MFI ratio, calculated as described in the materials and methods section. For ELISA, MOG-1-125 was bound to MaxiSorp plates and ΔOD was calculated after subtration of the OD of BSA coated MaxiSorp plates (**A**). Alternatively, MOG-1-125 was biotinylated at its C-terminal Avi-tag and bound to streptavidin plates. For ELISA, the anti-MOG reactivity is expressed as ΔOD (streptavidin + MOG) – (streptavidin only) (**B**). The horizontal dashed lines represent the mean of the anti-MOG reactivity of a total of 87 healthy controls + 3SDs. The vertical dashed lines represent the mean + 3SDs of 13 healthy controls. Samples included in the analysis of recognition of MOG-variants are shown with filled circles.

Fig. 2: Localization of the C-terminus of MOG. A) Schematic representation of the binding of the recombinant humanized r8-18C5 (blue) and ab28766 (yellow). **B)** Localization of the C-terminus of MOG. In the upper row (**B-E**), HeLa cells were transiently transfected with EYFP alone (closed grey graph), with FL-MOG (vermillion line), or ED-MOG (light blue line). FL-MOG and ED-MOG were fused to EYFP at the N-terminus. These cells were tested live (**B, D**) as well as after fixation and permeabilization (**C, E**) with r8-18C5 (**B, C**) and ab28766 (**D, E**). Gates were set to an EYFP signal >100. In the lower row (**F-I**), TE671 cells stably transfected with FL-MOG (vermillion line) or the empty vector (closed grey graph) were tested live (**F, H**) as well as after fixation and permeabilization (**G, I**) with r8-18C5 (**F, G**) and ab28766 (**H, I**). MFI values are given for each histogram.

Fig. 3: Detection of MOG-1-125 displayed on lipid-coated beads. A) Schematic representation of the lipid coated silica beads model. Glass bead of 6 μm in diameter were coated with a lipid mixture that formed a bilayer. The correctly folded MOG-1-125 is displayed on this bilayer. The magnification shows a segment of a single lipid coated bead. MOG-1-125 biotinylated is attached to the Biotinyl CAP PE via one of the free subunits of the neutravidin. MOG-1-125 is bound by the r8-18C5 (blue), which is detected by the Alexa Fluor 647 anti human IgG (magenta).

B, C) Confocal microscopy image of lipid coated beads, to asses the extent of the coating. **B)** The Atto488 DOPE lipids gave green fluorescence to the whole membrane coating. **C)** MOG displayed on these beads is detected by r8-18C5 and visualized with a red-labelled secondary antibody. **B+C** were taken with a 40X water objective; scale bar indicates 10 µm. **D)** Detection of increasing concentrations of r8-18C5 by cells transfected with FL-MOG (vermillion), ED-MOG (light blue line) and by lipid-coated beads displaying MOG-1-125 (dark green line). **E)** Binding of sera (diluted 1:50) of five patients with MOG-Abs to MOG-1-125 coated beads. The closed gray graphs represent background-bindings of the beads, the black line represents binding to beads displaying MOG-1-125. MFI values for each histogram are given.

Fig. 4: MOG variants used for transient transfection and their recognition by selected patients. The upper row shows cartoons of MOG-variants used. Rows 2-5 show dot-plots obtained with serum diluted 1:50 of the indicated patients. Patients #14, #5, and #7 represent the majority of the patients, because they show a greater recognition of FL-MOG compared to ED-MOG. Patient #22 has an unusual binding behavior, since it strongly recognizes ED-MOG. The lowest row shows the reactivity of the MOG-specific control mAb r8-18C5 (0.5 µg/ml). The two vertical lines in each dot-plot indicate an EGFP intensity of 100-500 (dotted one) that is used as threshold for the quantitative analysis in **Fig. 5**.

Fig. 5: Differential detection of MOG variants and quantification. A) Sera from 14 patients with MOG-Abs and one negative control (C) were tested for reactivity towards the six MOG-variants. The mAb r8-18C5 (0.5 µg/ml) was used as a control. For the quantitative evaluation, the cells with EGFP signal between 100-500 were considered (**Fig. 4**). Error bars indicate SEM of 2 experiments. **B)** The reactivity of all the MOG variants normalized to FL-MOG (set as 100%) is shown with EGFP gating of 100-500. ED-MOG, MOG-Cyt and opossum-MOG were significantly less capable to detect the MOG+ patients when compared to FL-MOG, MOG-2TMD and human-opossum-MOG ($p<0.0001$). The EGFP gating of 100-500 highlights also a difference in the reactivity between MOG-2TMD and FL-MOG ($p<0.05$), but MOG-2TMD is still capable of detecting all 14 MOG+ patients.

Fig. 6: Recognition of FL-MOG and ED-MOG by F(ab')2 and Fab preparations. A) Preparation of F(ab')2 and Fab. IgGs purified with protein-G columns were digested with pepsin to obtain the F(ab')2 and with papain to yield Fab. Since the Fab preparations obtained after papain digestion still contained undigested IgG, the Fab fragments were further purified by size exclusion chromatography (SEC). Elution fractions were separated by non-reducing SDS-PAGE and stained with Coomassie. Relevant elution fractions were then pooled and analyzed again on an SDS-PAGE gel. Here, #14 is shown as a representative example. **B)** HeLa cells were transfected with EGFP, FL-MOG or ED-MOG. Binding of IgGs from plasma (400 µg/ml), F(ab')2 (800 µg/ml) and Fab (800 µg/ml) of the indicated patients was determined with secondary antibodies specific for Ig-kappa and Ig-lambda as described in the materials and methods section. The mAb r8-18C5 (0.1 µg/ml) was used as a control. The anti-MOG reactivities were calculated on transfected cells with EGFP signal >500. MFI values are given for each histogram. Representative measurements from two experiments with similar results are shown.

Fig. 7: Model illustrating how the second hydrophobic domain of MOG enhances recognition of its extracellular part by autoantibodies from patients. We show in this paper that MOG-Abs from patients require bivalent binding and the second hydrophobic domain for MOG binding. We therefore propose the model shown here in which the second hydrophobic domain of MOG facilitates bivalent binding of MOG-Abs. The magnified figure shows how the second hydrophobic domain is embedded in the membrane in a homotypic manner with both sides of this hydrophobic domain in the cytoplasm. The two prolines (P) in the middle induce kinks inside the membrane. Positively charged amino acids arginine (R) and lysine (K) adjacent to the hydrophobic domain might interact with the cytosolic interface of the membrane. The cysteine (C) at the end of the hydrophobic domain might by palmitoylated. The presence of the second hydrophobic domain brings MOG molecules to a distance that allows bivalent binding of autoantibodies. The absence of the second hydrophobic domain in the ED-MOG protein leads to the weak and monovalent binding of MOG-Abs.

9. Reference list

Aoki S, Thomas A, Decaffmeyer M, Brasseur R, Epand RM. The role of proline in the membrane re-entrant helix of caveolin-1. J Biol Chem 2010; 285(43): 33371-80.

Bradl M, Misu T, Takahashi T, Watanabe M, Mader S, Reindl M*, et al.* Neuromyelitis optica: Pathogenicity of patient immunoglobulin in vivo. Annals of Neurology 2009; 66 630-43.

Brändle SM, Obermeier B, Senel M, Bruder J, Mentele R, Khademi M*, et al.* Distinct oligoclonal band antibodies in multiple sclerosis recognize ubiquitous self-proteins. Proc Natl Acad Sci U S A 2016; 113(28): 7864-9.

Brehm U, Piddlesden SJ, Gardinier MV, Linington C. Epitope specificity of demyelinating monoclonal autoantibodies directed against the human myelin oligodendrocyte glycoprotein (MOG). Journal of neuroimmunology 1999; 97(1-2): 9-15.

Breithaupt C, Schafer B, Pellkofer H, Huber R, Linington C, Jacob U. Demyelinating myelin oligodendrocyte glycoprotein-specific autoantibody response is focused on one dominant conformational epitope region in rodents. J Immunol 2008; 181(2): 1255-63.

Breithaupt C, Schubart A, Zander H, Skerra A, Huber R, Linington C*, et al.* Structural insights into the antigenicity of myelin oligodendrocyte glycoprotein. Proceedings of the National Academy of Sciences of the United States of America 2003; 100(16): 9446-51.

Brilot F, Dale RC, Selter RC, Grummel V, Kalluri SR, Aslam M*, et al.* Antibodies to native myelin oligodendrocyte glycoprotein in children with inflammatory demyelinating central nervous system disease. Ann Neurol 2009; 66(6): 833-42.

Brimberg L, Mader S, Fujieda Y, Arinuma Y, Kowal C, Volpe BT*, et al.* Antibodies as Mediators of Brain Pathology. Trends in immunology 2015; 36(11): 709-24.

Clements CS, Reid HH, Beddoe T, Tynan FE, Perugini MA, Johns TG*, et al.* The crystal structure of myelin oligodendrocyte glycoprotein, a key autoantigen in multiple sclerosis. Proc Natl Acad Sci U S A 2003; 100(19): 11059-64.

Crane JM, Lam C, Rossi A, Gupta T, Bennett JL, Verkman AS. Binding affinity and specificity of neuromyelitis optica autoantibodies to aquaporin-4 M1/M23 isoforms and orthogonal arrays. J Biol Chem 2011; 286(18): 16516-24.

Dale RC, Tantsis EM, Merheb V, Kumaran RY, Sinmaz N, Pathmanandavel K*, et al.* Antibodies to MOG have a demyelination phenotype and affect oligodendrocyte cytoskeleton. Neurol Neuroimmunol Neuroinflamm 2014; 1(1): e12.

Dalmau J, Graus F. Antibody-Mediated Encephalitis. N Engl J Med 2018; 378(9): 840-51.

della Gaspera B, Pham-Dinh D, Roussel G, Nussbaum JL, Dautigny A. Membrane topology of the myelin/oligodendrocyte glycoprotein. European journal of biochemistry 1998; 258(2): 478-84.

Diebolder CA, Beurskens FJ, de Jong RN, Koning RI, Strumane K, Lindorfer MA*, et al.* Complement is activated by IgG hexamers assembled at the cell surface. Science 2014; 343(6176): 1260-3.

Durozard P, Rico A, Boutiere C, Maarouf A, Lacroix R, Cointe S*, et al.* Comparison of the Response to Rituximab between Myelin Oligodendrocyte Glycoprotein and Aquaporin-4 Antibody Diseases. Ann Neurol 2020; 87(2): 256-66.

Flach AC, Litke T, Strauss J, Haberl M, Gomez CC, Reindl M*, et al.* Autoantibody-boosted T-cell reactivation in the target organ triggers manifestation of autoimmune CNS disease. Proc Natl Acad Sci U S A 2016; 113(12): 3323-8.

Fossati-Jimack L, Reininger L, Chicheportiche Y, Clynes R, Ravetch JV, Honjo T*, et al.* High pathogenic potential of low-affinity autoantibodies in experimental autoimmune hemolytic anemia. J Exp Med 1999; 190(11): 1689-96.

Fujihara K. Neuromyelitis optica spectrum disorders: still evolving and broadening. Curr Opin Neurol 2019; 32(3): 385-94.

Genain CP, Nguyen MH, Letvin NL, Pearl R, Davis RL, Adelman M*, et al.* Antibody facilitation of multiple sclerosis-like lesions in a nonhuman primate. The Journal of clinical investigation 1995; 96(6): 2966-74.

Gielen E, Smisdom N, De Clercq B, Vandeven M, Gijsbers R, Debyser Z*, et al.* Diffusion of myelin oligodendrocyte glycoprotein in living OLN-93 cells investigated by raster-scanning image correlation spectroscopy (RICS). Journal of fluorescence 2008; 18(5): 813-9.

Gielen E, Vercammen J, Sýkora J, Humpolickova J, Vandeven M, Benda A*, et al.* Diffusion of sphingomyelin and myelin oligodendrocyte glycoprotein in the membrane of OLN-93 oligodendroglial cells studied by fluorescence correlation spectroscopy. Comptes rendus biologies 2005; 328(12): 1057-64.

Hoftberger R, Guo Y, Flanagan EP, Lopez-Chiriboga AS, Endmayr V, Hochmeister S*, et al.* The pathology of central nervous system inflammatory demyelinating disease accompanying myelin oligodendrocyte glycoprotein autoantibody. Acta Neuropathol 2020.

Jarius S, Metz I, König FB, Ruprecht K, Reindl M, Paul F*, et al.* Screening for MOG-IgG and 27 other anti-glial and anti-neuronal autoantibodies in 'pattern II multiple sclerosis' and brain biopsy findings in a MOG-IgG-positive case. Mult Scler 2016; 22: 1541-9.

Jurynczyk M, Messina S, Woodhall MR, Raza N, Everett R, Roca-Fernandez A*, et al.* Clinical presentation and prognosis in MOG-antibody disease: a UK study. Brain 2017; 140(12): 3128-38.

Kim T, Pfeiffer SE. Myelin glycosphingolipid/cholesterol-enriched microdomains selectively sequester the non-compact myelin proteins CNP and MOG. Journal of neurocytology 1999; 28(4-5): 281-93.

Kinzel S, Lehmann-Horn K, Torke S, Hausler D, Winkler A, Stadelmann C*, et al.* Myelin-reactive antibodies initiate T cell-mediated CNS autoimmune disease by opsonization of endogenous antigen. Acta Neuropathol 2016; 132(1): 43-58.

Kortvelyessy P, Breu M, Pawlitzki M, Metz I, Heinze HJ, Matzke M*, et al.* ADEM-like presentation, anti-MOG antibodies, and MS pathology: TWO case reports. Neurol Neuroimmunol Neuroinflamm 2017; 4(3): e335.

Kroepfl JF, Viise LR, Charron AJ, Linington C, Gardinier MV. Investigation of myelin/oligodendrocyte glycoprotein membrane topology. J Neurochem 1996; 67(5): 2219-22.

Linington C, Bradl M, Lassmann H, Brunner C, Vass K. Augmentation of demyelination in rat acute allergic encephalomyelitis by circulating mouse monoclonal antibodies directed against a myelin/oligodendrocyte glycoprotein. Am J Pathol 1988; 130(3): 443-54.

Litzenburger T, Fässler R, Bauer J, Lassmann H, Linington C, Wekerle H*, et al.* B lymphocytes producing demyelinating autoantibodies: development and function in gene-targeted transgenic mice. The Journal of experimental medicine 1998; 188(1): 169-80.

Lucchinetti CF, Mandler RN, McGavern D, Br□ck W, Gleich G, Ransohoff RM*, et al.* A role for humoral mechanisms in the pathogenesis of Devic's neuromyelitis optica. Brain 2002; 125(Pt 7): 1450-61.

Ludwig RJ, Vanhoorelbeke K, Leypoldt F, Kaya Z, Bieber K, McLachlan SM*, et al.* Mechanisms of Autoantibody-Induced Pathology. Front Immunol 2017; 8: 603.

Mader S, Gredler V, Schanda K, Rostasy K, Dujmovic I, Pfaller K*, et al.* Complement activating antibodies to myelin oligodendrocyte glycoprotein in neuromyelitis optica and related disorders. J Neuroinflammation 2011; 8: 184.

Mader S, Kumpfel T, Meinl E. Novel insights into pathophysiology and therapeutic possibilities reveal further differences between AQP4-IgG- and MOG-IgG-associated diseases. Curr Opin Neurol 2020; 33(3): 362-71.

Marta CB, Montano MB, Taylor CM, Taylor AL, Bansal R, Pfeiffer SE. Signaling cascades activated upon antibody cross-linking of myelin oligodendrocyte glycoprotein: potential implications for multiple sclerosis. J Biol Chem 2005; 280(10): 8985-93.

Marti Fernandez I, Macrini C, Krumbholz M, Hensbergen PJ, Hipgrave Ederveen AL, Winklmeier S*, et al.* The Glycosylation Site of Myelin Oligodendrocyte Glycoprotein Affects Autoantibody Recognition in a Large Proportion of Patients. Front Immunol 2019; 10: 1189.

Mayer MC, Breithaupt C, Reindl M, Schanda K, Rostasy K, Berger T*, et al.* Distinction and temporal stability of conformational epitopes on myelin oligodendrocyte glycoprotein recognized by patients with different inflammatory central nervous system diseases. J Immunol 2013; 191(7): 3594-604.

McLaughlin KA, Chitnis T, Newcombe J, Franz B, Kennedy J, McArdel S*, et al.* Age-dependent B cell autoimmunity to a myelin surface antigen in pediatric multiple sclerosis. J Immunol 2009; 183(6): 4067-76.

Nilsson I, Saaf A, Whitley P, Gafvelin G, Waller C, von Heijne G. Proline-induced disruption of a transmembrane alpha-helix in its natural environment. J Mol Biol 1998; 284(4): 1165-75.

O'Connor KC, McLaughlin KA, De Jager PL, Chitnis T, Bettelli E, Xu C*, et al.* Self-antigen tetramers discriminate between myelin autoantibodies to native or denatured protein. Nat Med 2007; 13(2): 211-7.

Perera NC, Wiesmuller KH, Larsen MT, Schacher B, Eickholz P, Borregaard N*, et al.* NSP4 is stored in azurophil granules and released by activated neutrophils as active endoprotease with restricted specificity. J Immunol 2013; 191(5): 2700-7.

Peschl P, Schanda K, Zeka B, Given K, Bohm D, Ruprecht K*, et al.* Human antibodies against the myelin oligodendrocyte glycoprotein can cause complement-dependent demyelination. J Neuroinflammation 2017; 14(1): 208.

Pittock SJ, Berthele A, Fujihara K, Kim HJ, Levy M, Palace J*, et al.* Eculizumab in Aquaporin-4-Positive Neuromyelitis Optica Spectrum Disorder. N Engl J Med 2019; 381(7): 614-25.

Pollinger B, Krishnamoorthy G, Berer K, Lassmann H, Bosl MR, Dunn R*, et al.* Spontaneous relapsing-remitting EAE in the SJL/J mouse: MOG-reactive transgenic T cells recruit endogenous MOG-specific B cells. The Journal of experimental medicine 2009; 206(6): 1303-16.

Pröbstel AK, Dornmair K, Bittner R, Sperl P, Jenne D, Magalhaes S*, et al.* Antibodies to MOG are transient in childhood acute disseminated encephalomyelitis. Neurology 2011; 77(6): 580-8.

Ramm B, Glock P, Mucksch J, Blumhardt P, Garcia-Soriano DA, Heymann M*, et al.* The MinDE system is a generic spatial cue for membrane protein distribution in vitro. Nat Commun 2018; 9(1): 3942.

Reindl M, Schanda K, Woodhall M, Tea F, Ramanathan S, Sagen J*, et al.* International multicenter examination of MOG antibody assays. 2020; 7(2).

Reindl M, Waters P. Myelin oligodendrocyte glycoprotein antibodies in neurological disease. Nat Rev Neurol 2019; 15(2): 89-102.

Saadoun S, Waters P, Owens GP, Bennett JL, Vincent A, Papadopoulos MC. Neuromyelitis optica MOG-IgG causes reversible lesions in mouse brain. Acta Neuropathol Commun 2014; 2(1): 35.

Shaw A, Hoffecker IT, Smyrlaki I, Rosa J, Grevys A, Bratlie D*, et al.* Binding to nanopatterned antigens is dominated by the spatial tolerance of antibodies. Nat Nanotechnol 2019; 14(2): 184-90.

Sinmaz N, Nguyen T, Tea F, Dale RC, Brilot F. Mapping autoantigen epitopes: molecular insights into autoantibody-associated disorders of the nervous system. J Neuroinflammation 2016; 13(1): 219.

Smotrys JE, Linder ME. Palmitoylation of intracellular signaling proteins: regulation and function. Annu Rev Biochem 2004; 73: 559-87.

Smulski CR, Decossas M, Chekkat N, Beyrath J, Willen L, Guichard G*, et al.* Hetero-oligomerization between the TNF receptor superfamily members CD40, Fas and TRAILR2 modulate CD40 signalling. Cell Death Dis 2017; 8(2): e2601.

Soltys J, Liu Y, Ritchie A, Wemlinger S, Schaller K, Schumann H*, et al.* Membrane assembly of aquaporin-4 autoantibodies regulates classical complement activation in neuromyelitis optica. J Clin Invest 2019; 129(5): 2000-13.

Spadaro M, Gerdes LA, Mayer MC, Ertl-Wagner B, Laurent S, Krumbholz M*, et al.* Histopathology and clinical course of MOG-antibody associated encephalomyelitis. Annals of Clinical and Translational Neurology 2015; 2: 295-301.

Spadaro M, Winklmeier S, Beltran E, Macrini C, Hoftberger R, Schuh E*, et al.* Pathogenicity of human antibodies against myelin oligodendrocyte glycoprotein. Ann Neurol 2018; 84(2): 315-28.

Stryer L, Haugland RP. Energy transfer: a spectroscopic ruler. Proc Natl Acad Sci U S A 1967; 58(2): 719-26.

Takai Y, Misu T, Kaneko K, Chihara N, Narikawa K, Tsuchida S*, et al.* Myelin oligodendrocyte glycoprotein antibody-associated disease: an immunopathological study. Brain 2020; 143(5): 1431-46.

Tea F, Lopez JA, Ramanathan S, Merheb V, Lee FXZ, Zou A*, et al.* Characterization of the human myelin oligodendrocyte glycoprotein antibody response in demyelination. Acta Neuropathol Commun 2019; 7(1): 145.

von Heijne G. Proline kinks in transmembrane alpha-helices. J Mol Biol 1991; 218(3): 499-503.

Waters P, Woodhall M, O'Connor KC, Reindl M, Lang B, Sato DK*, et al.* MOG cell-based assay detects non-MS patients with inflammatory neurologic disease. Neurol Neuroimmunol Neuroinflamm 2015; 2(3): e89.

Weber MS, Derfuss T, Metz I, Bruck W. Defining distinct features of anti-MOG antibody associated central nervous system demyelination. Ther Adv Neurol Disord 2018; 11: 1756286418762083.

Winklmeier S, Schluter M, Spadaro M, Thaler FS, Vural A, Gerhards R*, et al.* Identification of circulating MOG-specific B cells in patients with MOG antibodies. Neurol Neuroimmunol Neuroinflamm 2019; 6(6): 625.

Zamvil SS, Slavin AJ. Does MOG Ig-positive AQP4-seronegative opticospinal inflammatory disease justify a diagnosis of NMO spectrum disorder? Neurol Neuroimmunol Neuroinflamm 2015; 2(1): e62.

Zhou R, Yang G, Guo X, Zhou Q, Lei J, Shi Y. Recognition of the amyloid precursor protein by human gamma-secretase. Science 2019; 363(6428).

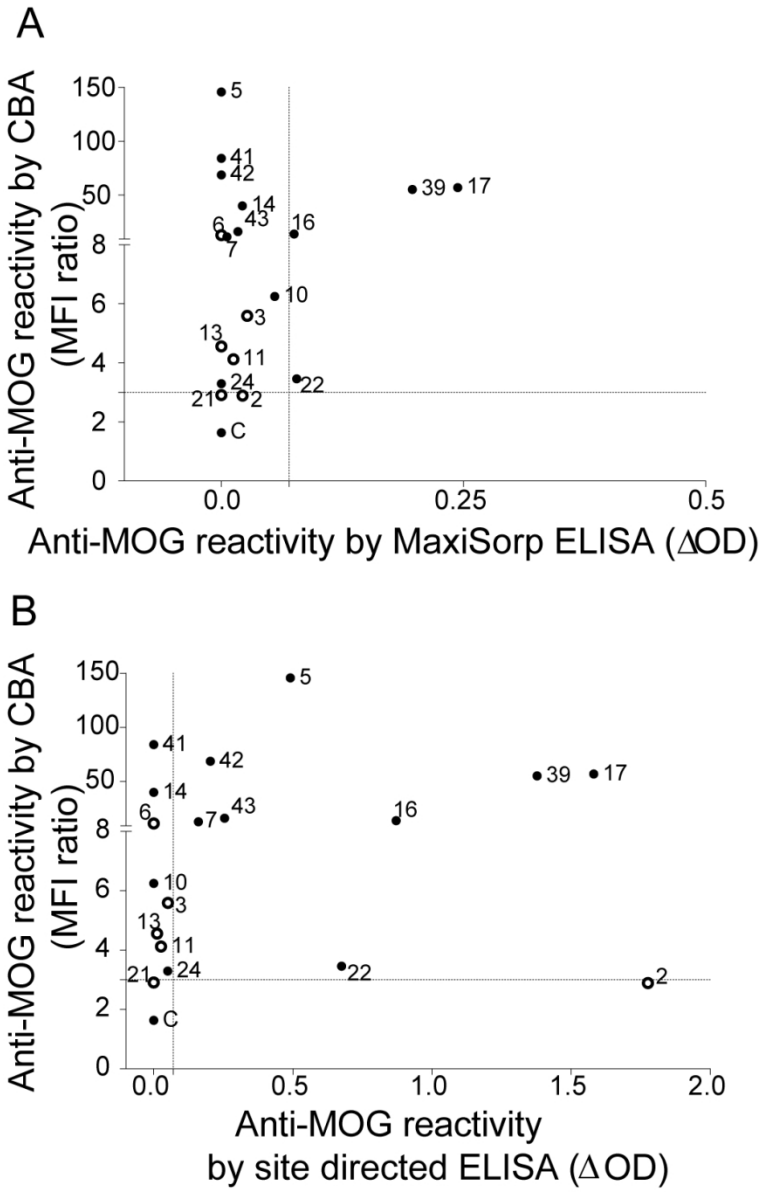

Fig. 1: Comparison of MOG-reactivity by ELISA and cell-based assay (CBA). The anti-MOG-reactivity of 18 patients with MOG-Abs was determined by CBA using FL-MOG and by ELISA. CBA was performed as described (Spadaro et al., 2018) and the anti-MOG reactivity is shown as MFI ratio, calculated as described in the materials and methods section. For ELISA, MOG-1-125 was bound to MaxiSorp plates and a delta OD was calculated after substration of the OD of BSA coated MaxiSorp plates (A). Alternatively, MOG-1-125 was biotinylated at its C-terminal Avi-tag and bound to streptavidin plates. For ELISA, the anti-MOG reactivity is expressed as ΔOD (streptavidin + MOG) – (streptavidin only) (B). The horizontal dashed lines represent the mean of the anti-MOG reactivity of a total of 87 healthy controls + 3SDs. The vertical dashed lines represent the mean + 3SDs of 13 healthy controls. Samples included in the analysis of recognition of MOG-variants are shown with filled circles.

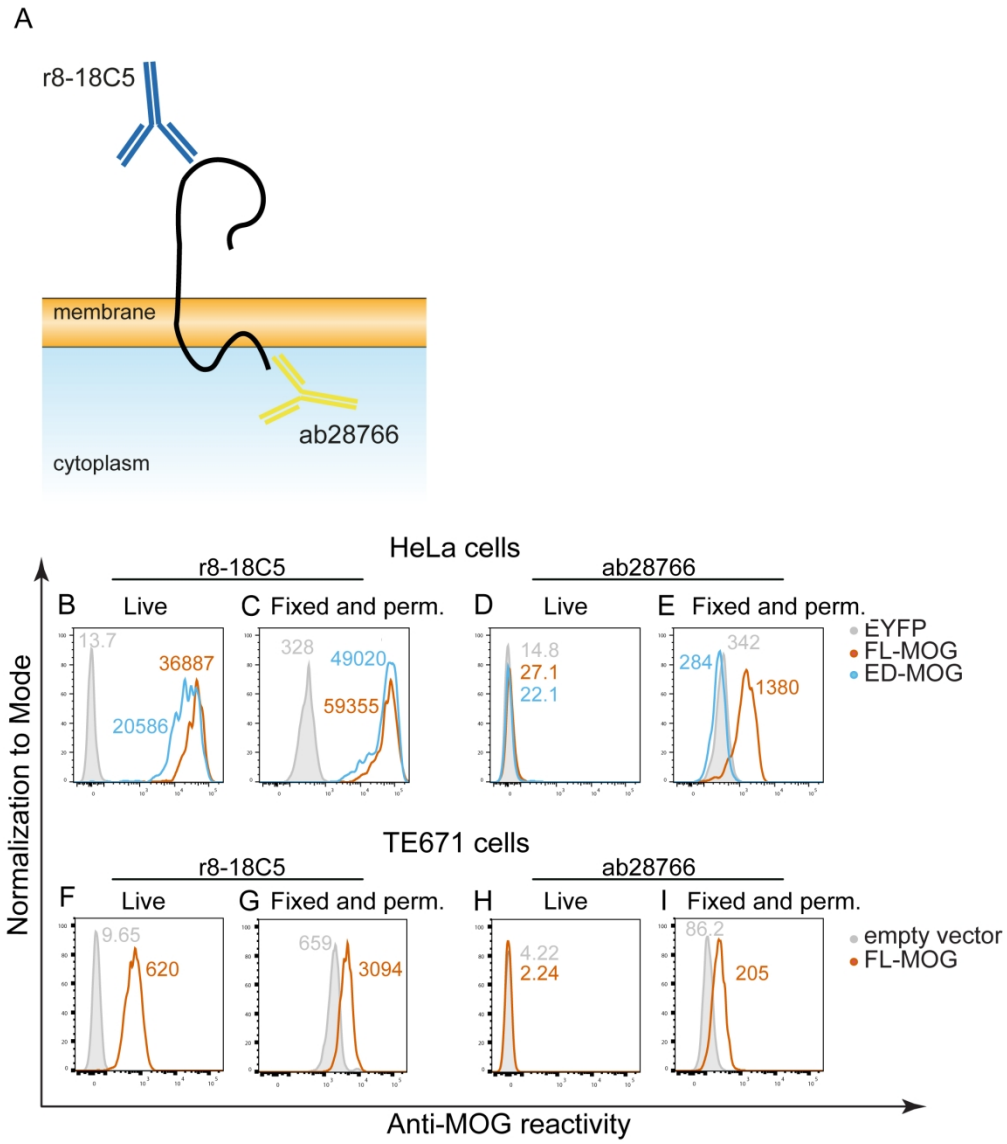

Fig. 2: Localization of the C-terminus of MOG. A) Schematic representation of the binding of the recombinant humanized r8-18C5 (blue) and ab28766 (yellow). B) Localization of the C-terminus of MOG. In the upper row (B-E), HeLa cells were transiently transfected with EYFP alone (closed grey graph), with FL-MOG (vermillion line), or ED-MOG (light blue line). FL-MOG and ED-MOG were fused to EYFP at the N-terminus. These cells were tested live (B, D) as well as after fixation and permeabilization (C, E) with r8-18C5 (B, C) and ab28766 (D, E). Gates were set to an EYFP signal >100. In the lower row (F-I), TE671 cells stably transfected with FL-MOG (vermillion line) or the empty vector (closed grey graph) were tested live (F, H) as well as after fixation and permeabilization (G, I) with r8-18C5 (F, G) and ab28766 (H, I). MFI values are given for each histogram.

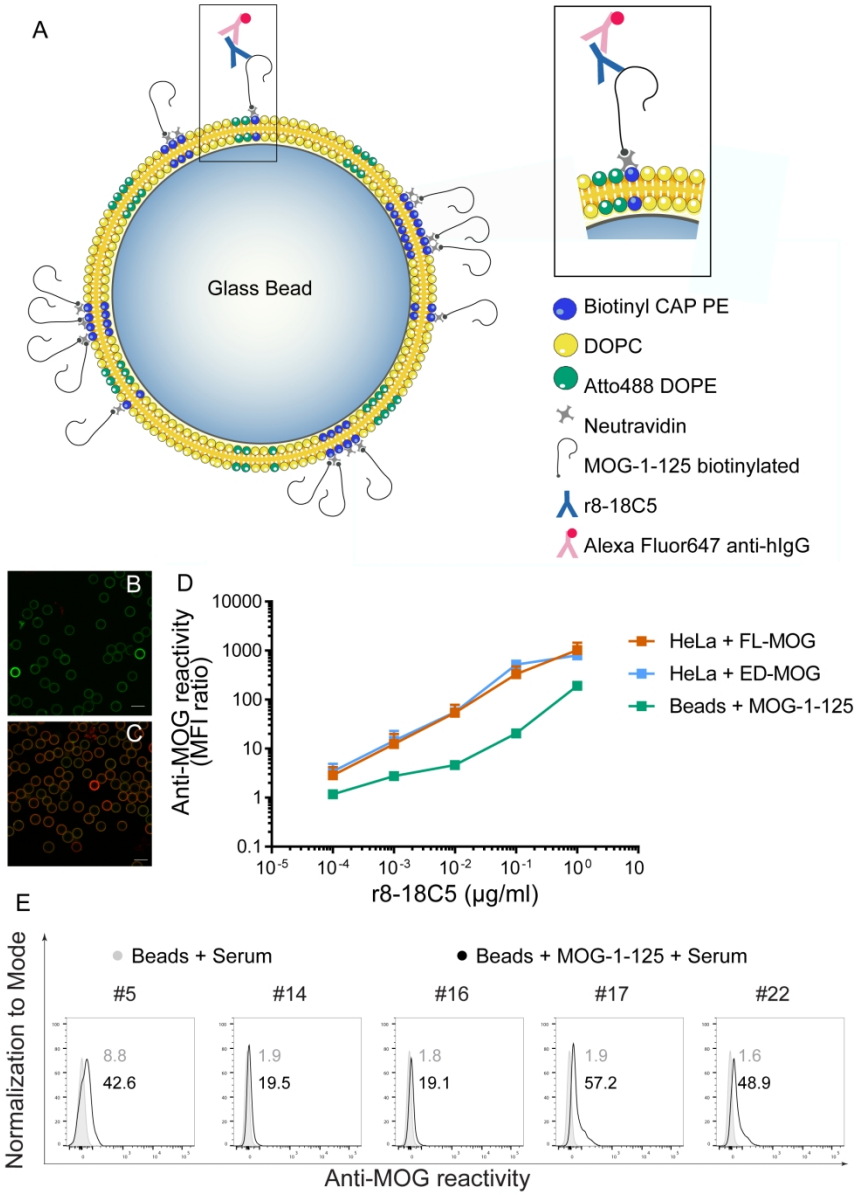

Fig. 3: Detection of MOG-1-125 displayed on lipid-coated beads. A) Schematic representation of the lipid coated silica beads model. Glass bead of 6 µm in diameter were coated with a lipid mixture that formed a bilayer. The correctly folded MOG-1-125 is displayed on this bilayer. The magnification shows a segment of a single lipid coated bead. MOG-1-125 biotinylated is attached to the Biotinyl CAP PE via one of the free subunits of the neutravidin. MOG-1-125 is bound by the r8-18C5 (blue), which is detected by the Alexa Fluor 647 anti human IgG (magenta). B, C) Confocal microscopy image of lipid coated beads, to asses the extent of the coating. B) The Atto488 DOPE lipids gave green fluorescence to the whole membrane coating. C) MOG displayed on these beads is detected by r8-18C5 and visualized with a red-labelled secondary antibody. B+C were taken with a 40X water objective; scale bar indicates 10 µm. D) Detection of increasing concentrations of r8-18C5 by cells transfected with FL-MOG (vermillion), ED-MOG (light blue line) and by lipid-coated beads displaying MOG-1-125 (dark green line). E) Binding of sera (diluted 1:50) of five patients with MOG-Abs to MOG-1-125 coated beads. The closed gray graphs represent background-bindings of the beads, the black line represents binding to beads displaying MOG-1-125. MFI values for each histogram are given.

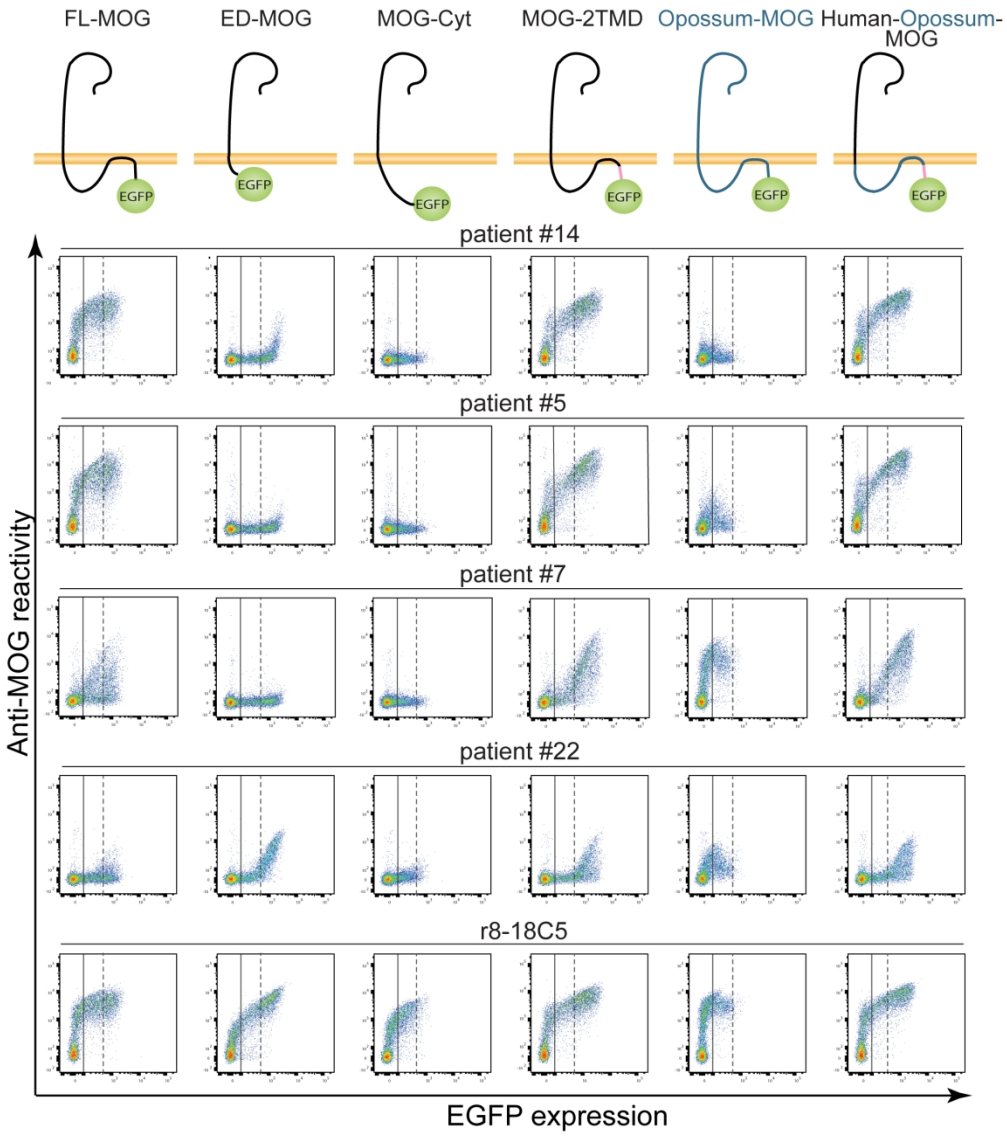

Fig. 4: MOG variants used for transient transfection and their recognition by selected patients. The upper row shows cartoons of MOG-variants used. Rows 2-5 show dot-plots obtained with serum diluted 1:50 of the indicated patients. Patients #14, #5, and #7 represent the majority of the patients, because they show a greater recognition of FL-MOG compared to ED-MOG. Patient #22 has an unusual binding behavior, since it strongly recognizes ED-MOG. The lowest row shows the reactivity of the MOG-specific control mAb r8-18C5 (0.5 µg/ml). The two vertical lines in each dot-plot indicate an EGFP intensity of 100-500 (dotted one) that is used as threshold for the quantitative analysis in Fig. 5.

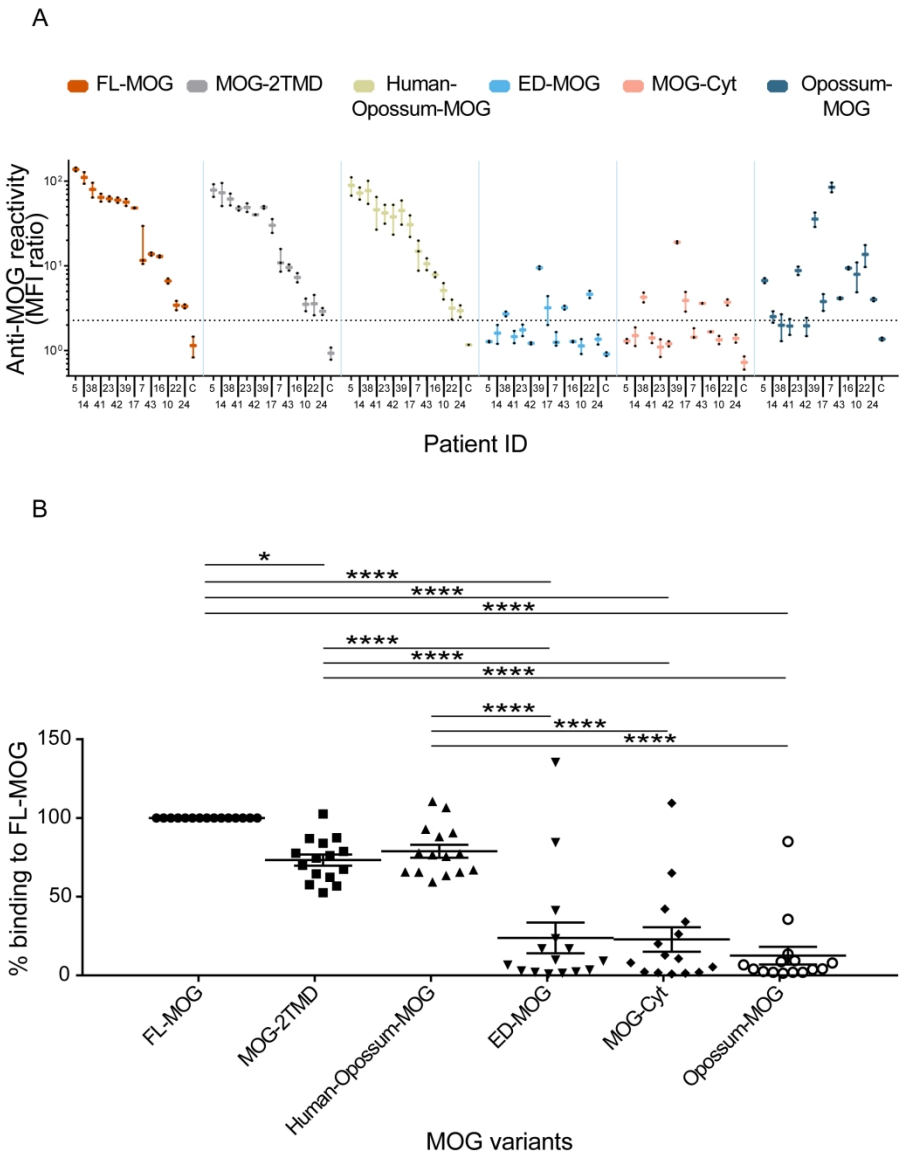

Fig. 5: Differential detection of MOG variants and quantification. A) Sera from 14 patients with MOG-Abs and one negative control (C) were tested for reactivity towards the six MOG-variants. The mAb r8-18C5 (0.5 µg/ml) was used as a control. For the quantitative evaluation, the cells with EGFP signal between 100-500 were considered (Fig. 4). Error bars indicate SEM of 2 experiments. B) The reactivity of all the MOG variants normalized to FL-MOG (set as 100%) is shown with EGFP gating of 100-500. ED-MOG, MOG-Cyt and opossum-MOG were significantly less capable to detect the MOG+ patients when compared to FL-MOG, MOG-2TMD and human-opossum-MOG ($p<0.0001$). The EGFP gating of 100-500 highlights also a difference in the reactivity between MOG-2TMD and FL-MOG ($p<0.05$), but MOG-2TMD is still capable of detecting all 14 MOG+ patients.

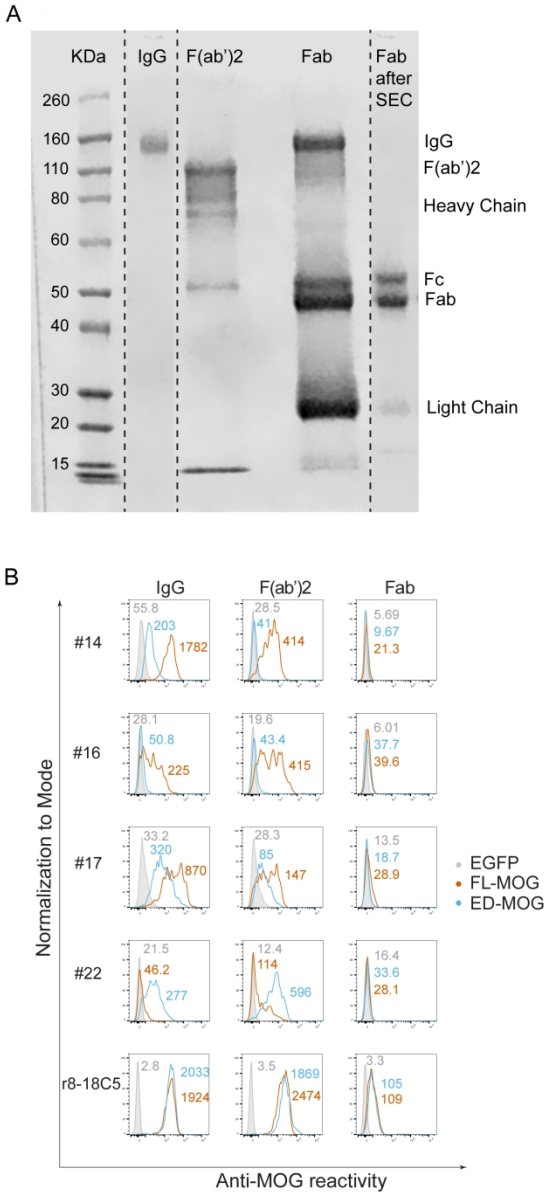

Fig. 6: Recognition of FL-MOG and ED-MOG by F(ab')2 and Fab preparations. A) Preparation of F(ab')2 and Fab. IgGs purified with protein-G columns were digested with pepsin to obtain the F(ab')2 and with papain to yield Fab. Since the Fab preparations obtained after papain digestion still contained undigested IgG, the Fab fragments were further purified by size exclusion chromatography (SEC). Elution fractions were separated by non-reducing SDS-PAGE and stained with Coomassie. Relevant elution fractions were then pooled and analyzed again on an SDS-PAGE gel. Here, #14 is shown as a representative example. B) HeLa cells were transfected with EGFP, FL-MOG or ED-MOG. Binding of IgGs from plasma (400 µg/ml), F(ab')2 (800 µg/ml) and Fab (800 µg/ml) of the indicated patients was determined with secondary antibodies specific for Ig-kappa and Ig-lambda as described in the materials and methods section. The mAb r8-18C5 (0.1 µg/ml) was used as a control. The anti-MOG reactivities were calculated on transfected cells with EGFP signal >500. MFI values are given for each histogram. Representative measurements from two experiments with similar results are shown.

Figure 7

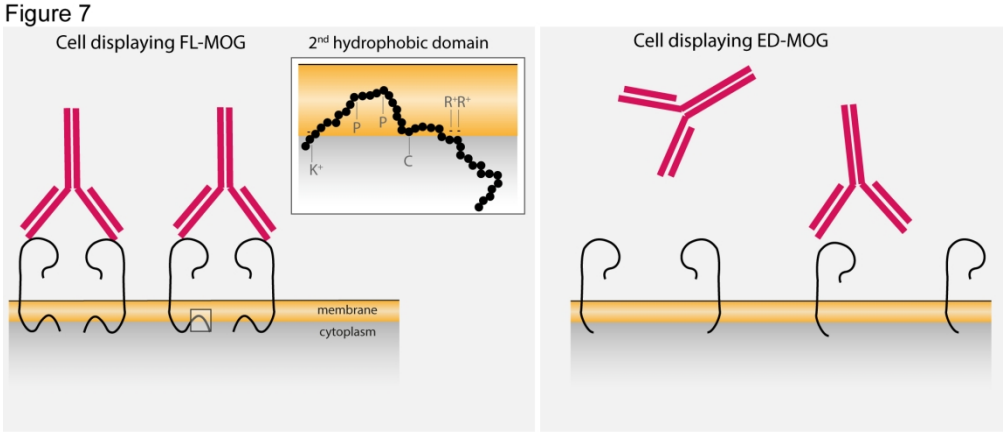

Fig. 7: Model illustrating how the second hydrophobic domain of MOG enhances recognition of its extracellular part by autoantibodies from patients. We show in this paper that MOG-Abs from patients require bivalent binding and the second hydrophobic domain for MOG binding. We therefore propose the model shown here in which the second hydrophobic domain of MOG facilitates bivalent binding of MOG-Abs. The magnified figure shows how the second hydrophobic domain is embedded in the membrane in a homotypic manner with both sides of this hydrophobic domain in the cytoplasm. The two prolines (P) in the middle induce kinks inside the membrane. Positively charged amino acids arginine (R) and lysine (K) adjacent to the hydrophobic domain might interact with the cytosolic interface of the membrane. The cysteine (C) at the end of the hydrophobic domain might by palmitoylated. The presence of the second hydrophobic domain brings MOG molecules to a distance that allows bivalent binding of autoantibodies. The absence of the second hydrophobic domain in the ED-MOG protein leads to the weak and monovalent binding of MOG-Abs.

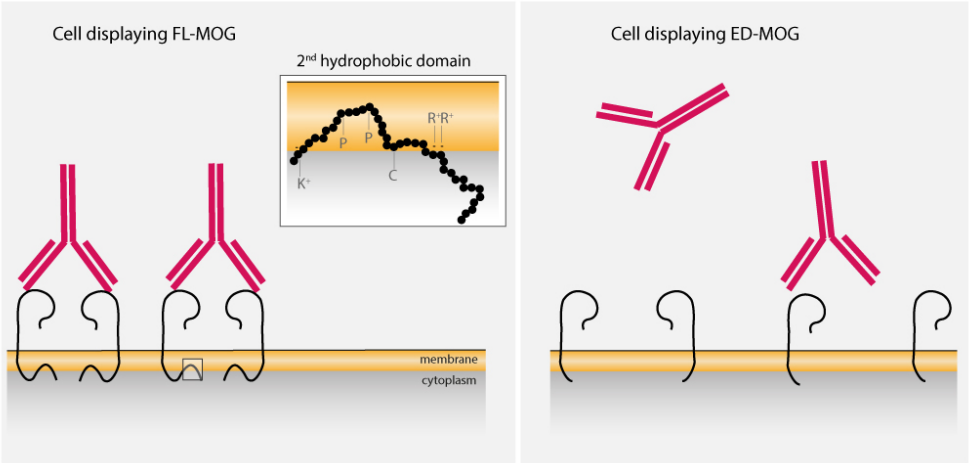

260x130mm (100 x 100 DPI)

Macrini *et al*. report that MOG-antibodies require the intracellular part of MOG and bivalent binding for MOG-recognition, explaining why a cell-based assay is needed to detect them. As bivalently bound antibodies bind only poorly to C1q, complement activation is probably not the major pathomechanism of MOG-antibodies.